MSFC-269

Effect of Oblique Electromagnetic Ion Cyclotron Waves on Relativistic Electron Scattering: CRRES Based Calculation

G. V. Khazanov

NASA, Marshall Space Flight Center, Huntsville, Alabama, USA

K. V. Gamayunov

NASA, Marshall Space Flight Center, Huntsville, Alabama, USA

Short title: RB ELECTRON SCATTERING BY EMIC WAVES

Abstract. We consider the effect of oblique EMIC waves on relativistic electron scattering in the outer radiation belt using simultaneous observations of plasma and wave parameters from CRRES. The main findings can be summarized as follows: 1. In comparison with field–aligned waves, intermediate and highly oblique distributions decrease the range of pitch–angles subject to diffusion, and reduce the local scattering rate by an order of magnitude at pitch–angles where the principle $|n| = 1$ resonances operate. Oblique waves allow the $|n| > 1$ resonances to operate, extending the range of local pitch–angle diffusion down to the loss cone, and increasing the diffusion at lower pitch–angles by orders of magnitude; 2. The local diffusion coefficients derived from CRRES data are qualitatively similar to the local results obtained for prescribed plasma/wave parameters. Consequently, it is likely that the bounce–averaged diffusion coefficients, if estimated from concurrent data, will exhibit the dependencies similar to those we found for model calculations; 3. In comparison with field–aligned waves, intermediate and highly oblique waves decrease the bounce–averaged scattering rate near the edge of the equatorial loss cone by orders of magnitude if the electron energy does not exceed a threshold ($\sim 2 - 5$ MeV) depending on specified plasma and/or wave parameters; 4. For greater electron energies, oblique waves operating the $|n| > 1$ resonances are more effective and provide the same bounce–averaged diffusion rate near the loss cone as field–aligned waves do.

1. Introduction

The flux of outer zone relativistic electrons (above 1 MeV) is extremely variable during geomagnetic storms. The competition between source and loss, both of which are enhanced during storm periods, determines the resulting relativistic electron flux level in the Earth's outer radiation belt (RB) [e. g., *Summers et al.*, 2004; *Reeves et al.*, 2003; *Green et al.*, 2004]. Usually, the flux falls by up to two or three orders of magnitude during main phase, and gradually increases over a period of a few days during storm recovery phase [e. g., *Meredith et al.*, 2002]. Analyzing 256 geomagnetic storms during the period 1989–2000, *Reeves et al.* [2003] found that 53 % of storms lead to higher flux during the storm recovery phase in comparison to pre–storm levels; 28 % produce no change; and 19 % lead to net decrease in flux. The large electron flux decrease during the main storm phase is usually associated with a decrease of *Dst* when the relativistic electrons adiabatically respond to the stretching of the magnetic field lines caused by the formation of a partial ring current (RC) [*Kim and Chan,* 1997], and/or a drift out the magnetopause boundary [*Li et al.,* 1997], and/or nonadiabatic scattering into the loss cone due to cyclotron interaction with electromagnetic ion cyclotron (EMIC) waves [*Thorne and Kennel,* 1971; *Lyons and Thorne,* 1972; *Summers and Thorne,* 2003; *Albert,* 2003; *Thorne et al.,* 2005] and/or whistler–mode chorus/hiss waves [e. g., *Summers et al.*, 2007].

Precipitation of outer RB electrons due to resonant pitch–angle scattering by EMIC waves is considered to be one of the most important loss mechanisms. Recently,

data from balloon–borne X–ray instruments provided indirect but strong evidence for the ability of EMIC waves to cause precipitation of outer zone relativistic electrons in the late afternoon–dusk MLT sector [*Foat et al.*, 1998; *Lorentzen et al.*, 2000; *Millan et al.*, 2002]. These observations stimulated theoretical and statistical studies which demonstrated that this mechanism of MeV electron pitch–angle diffusion can operate in the limit of strong diffusion, and can compete with adiabatic depletion caused by the *Dst* effect during the initial and main phases of storm [*Summers and Thorne*, 2003; *Albert*, 2003; *Loto'aniu et al.*, 2006; *Meredith et al.*, 2003].

Although the effectiveness of relativistic electron scattering depends strongly on EMIC wave spectral properties, unrealistic assumptions regarding the wave angular spread were made in previous theoretical studies. Namely, only strictly field–aligned or quasi field–aligned waves were considered as a driver for electron precipitation [e. g., *Summers and Thorne*, 2003; *Albert*, 2003; *Loto'aniu et al.*, 2006]. The effect of oblique EMIC waves on relativistic electron scattering was recently discussed by *Glauert and Horne* [2005]. For prescribed plasma and wave parameters, considering the H^+–mode EMIC waves, they calculated the equatorial diffusion coefficients and demonstrated that when a realistic angular spread of propagating waves is taken into account, electron diffusion at ~ 0.5 MeV is only slightly reduced compared with the assumption of field–aligned propagation, but at ~ 5 MeV, electron diffusion at pitch–angles near 90° is reduced by a factor of 5 and increased by several orders of magnitude at pitch–angles $30° - 80°$. As a result, EMIC waves should flatten the pitch–angle distribution.

Thus, at energies of a few MeV, the assumption of field–aligned propagation

breaks down, significantly overestimating the pitch–angle diffusion coefficient at large pitch–angles, while underestimating the local diffusion rate at smaller pitch–angles by orders of magnitude. This is a very strong effect, so in contrast to [*Glauert and Horne,* 2005], it is important to consider the impact of oblique EMIC waves on relativistic electron scattering using simultaneous observations for plasma/wave parameters, and to estimate the effect of bounce averaging. In the present study we calculate the pitch–angle diffusion coefficients using plasma and wave parameters observed by the Combined Release and Radiation Effects Satellite (CRRES) as reported by *Loto'aniu et al.* [2006].

This article is organized as follows: In section 2 we verify the pitch–angle diffusion coefficient calculations comparing our results with published results for both the equatorial and bounce–averaged scattering rates. Then, using model wave spectra for He^+–mode EMIC waves with defined plasma parameters, we consider the effect of the wave normal angle distribution on relativistic electron scattering. In section 3, using plasma/wave parameters observed by CRRES [*Loto'aniu et al.,* 2006], we present the results of our calculations and analysis of the local pitch–angle diffusion coefficients for two selected wave packets. Finally, in section 4 we summarize the main findings of our study.

2. Equatorial and Bounce–Averaged Pitch–Angle Diffusion Coefficients: Model Calculations

An extensive statistical analysis of the EMIC events presented by *Meredith et al.* [2003], showed that most of the cases when the minimum resonant electron energy fell below 2 MeV were associated with wave frequencies just below the He^+ gyrofrequency. So we take into account only the He^+–mode EMIC waves in the present study. The model wave frequency spectrum is assumed to be Gaussian,

$$B^2(\omega) \sim \exp\left\{-\frac{(\omega-\omega_m)^2}{\delta\omega^2}\right\}, \quad \omega_{LC} \le \omega \le \omega_{UC}, \tag{1}$$

where, following *Summers and Thorne* [2003] and/or *Albert* [2003], $\omega_{LC} = \omega_m - \delta\omega$, $\omega_{UC} = \omega_m + \delta\omega$, $\omega_m = 3\Omega_{O+}$, $\delta\omega = 0.5\Omega_{O+}$, and Ω_{O+} is the gyrofrequency of O^+. In our calculations, the wave normal angle distribution, $g(\theta)$, is assumed to be a constant inside a specified region and zero otherwise. Below we consider the following three cases,

$$\begin{aligned} \text{Case A (field}-\text{aligned)}: &\quad 0^\circ \le \theta < 30^\circ,\ 150^\circ < \theta \le 180^\circ, \\ \text{Case B (intermediate)}: &\quad 30^\circ \le \theta < 60^\circ,\ 120^\circ < \theta \le 150^\circ, \\ \text{Case C (oblique)}: &\quad 60^\circ \le \theta \le 89^\circ,\ 91^\circ \le \theta \le 120^\circ, \end{aligned} \tag{2}$$

where θ is the wave normal angle. Note that the diffusion coefficient is a linear functional of the wave spectral density, and the sum of cases A, B, and C describe a situation when EMIC wave energy is evenly distributed over the entire wave normal angle region $0^\circ \le \theta \le 180^\circ$ (we excluded the region near 90° because of Landau damping by thermal electrons [e. g., *Thorne and Horne,* 1992; *Khazanov et al.,* 2007]). For benchmark

purposes, we calculate also the diffusion coefficients for a Gaussian distribution over $x = \tan\theta$ ($0° \leq \theta \leq 15°$) which has been used by *Albert* [2003]. In each case, the wave amplitude is normalized to ensure

$$\int_{\omega_{LC}}^{\omega_{UC}} \mathrm{d}\omega \int_0^{\pi} \mathrm{d}\theta B^2(\omega)\, g(\theta) = 1\ \mathrm{nT}^2. \tag{3}$$

Finally, to specify the ion content we follow *Summers and Thorne* [2003], *Albert* [2003], *Meredith et al.* [2003], *Loto'aniu et al.* [2006], and prescribe the ion composition to be 70% H^+, 20% He^+, and 10% O^+ (following [*Meredith et al.,* 2003] we call it a "storm time" ion composition).

The results obtained using the relativistic version of the diffusion coefficient code of *Khazanov et al.* [2003] are shown in Figure 1. The first row shows the equatorial pitch–angle diffusion coefficients, the second row shows the corresponding resonance numbers averaged with the following weights:

Figure 1

$$\left\langle n(E,\alpha)\right\rangle = \frac{\sum_n n\left(\int_{\omega_{LC}}^{\omega_{UC}} \mathrm{d}\omega \int_0^{\pi} \mathrm{d}\theta D^n_{\alpha\alpha}(\omega,\theta,E,\alpha)\right)}{\sum_n \left(\int_{\omega_{LC}}^{\omega_{UC}} \mathrm{d}\omega \int_0^{\pi} \mathrm{d}\theta D^n_{\alpha\alpha}(\omega,\theta,E,\alpha)\right)}, \tag{4}$$

where E and α are the electron kinetic energy and local pitch–angle, and $D^n_{\alpha\alpha}(\omega,\theta,E,\alpha)$ is the partial equatorial pitch–angle diffusion coefficient, and the third row shows the bounce–averaged diffusion coefficients. Note that resonances $\pm n$ come together because the ω–term can be omitted in the quasilinear resonance condition, $\omega - k_{\|}v_{\|} - n\Omega_e/\gamma = 0$, [e. g., *Summers and Thorne,* 2003], and because the wave spectra are symmetric over $\theta = 90°$. The "Gauss" lines in Figure 1 show the results for a Gaussian distribution over x, and reproduce well the equatorial and bounce–averaged diffusion coefficients by *Albert* [2003, Figure 6].

Let us first analyze the equatorial pitch–angle diffusion coefficients. For all energies, Case A is only slightly less than "Gauss" if only $|n| = 1$ resonances operate, but in the region of $|n| > 1$ it is about 5 times greater (Figure 1(c) and 1(d), the first row). These dependencies are in good agreement with the previous results by *Albert* [2003, Figure 10, the second row]. For both "Gauss" and Case A, as follows from the second row in the Figure 1, the contributions from $n < 0$ are negligible compared to $n > 0$, especially for lower electron energies (see Figure 1(a) and 1(b), the second row). Cases B and C further increase the EMIC wave normal angle, and as a result, suppress the $|n| = 1$ resonances, and for low energies substantially shrink the region of pitch–angles subject to diffusion (see Figure 1(a) and 1(b), the first row). At the same time, they increase by orders of magnitude the contribution from $|n| > 1$, which operate for greater electron energies, and cover a greater pitch–angle region (see Figure 1(c) and 1(d), the first row). The growing contribution of the $n < 0$ resonances is more pronounced in Cases B and C (in comparison to Case A) because EMIC waves become more elliptically polarized with increasing wave normal angle (see Figure 1, the second row).

Overall, in comparison with the field–aligned waves, the intermediate and highly oblique wave distributions decrease the pitch–angle range subjected to diffusion, and reduce the equatorial scattering rate by orders of magnitude for low energy electrons ($E < 2$ MeV) when only principle $|n| = 1$ resonances operate. For greater electron energies, the $|n| = 1$ resonances operate only in a narrow region at large pitch-angles, and despite their greater contribution from field–aligned waves, cannot support the local electron diffusion into the loss cone. In this case, oblique waves operate on the $|n| > 1$

resonances more effectively, and extend the range of pitch–angle diffusion down to the loss cone. Note that despite our inclusion of the He^+–mode, the above results are in qualitative agreement with the results of *Glauert and Horne* [2005, Figures 6 and 7] obtained for the equatorial pitch–angle scattering by the H^+–mode EMIC waves.

Now we consider the effect of bounce averaging on pitch-angle diffusion coefficients. To calculate the bounce–averaged diffusion coefficients, we utilize all the plasma/wave parameters used in the above calculation of the equatorial coefficients, and in addition, a dipole magnetic field model, and the meridional density distribution from [*Khazanov et al.*, 2006]. We further assume that the EMIC waves are confined to mirror points, and the wave spectra are equatorial.

In all considered cases (2), the bounce averaging does not change the shape of the diffusion coefficients for energies below 2 MeV (compare the first and third rows in Figure 1) but simply reduces the pitch–angle diffusion rates by an order of magnitude. For energies 5 and 10 MeV, the peak values of the bounce–averaged diffusion coefficients are lower by about a factor of 3 than in the first row of Figure 1. However, the bounce–averaged results for $E > 2$ MeV differ qualitatively from the local coefficients for all wave normal distributions. Due to significant scattering at higher latitudes, the bounce–averaged diffusion coefficients extend further into the loss cone compared to equatorial results. The bounce–averaged results in Figure 1 demonstrate clearly the effect of EMIC wave normal angle distribution on relativistic electron scattering.

Recently, *Shprits et al.* [2006] showed that the electron lifetime is most sensitive to the value of the bounce–averaged scattering rate near the edge of the equatorial loss

cone, whose value is used to estimate the electron loss timescale [e. g., *Summers et al.*, 2007]. Considering the third row in Figures 1(a), 1(b), we can see that the intermediate and highly oblique wave distributions reduce the scattering rate near the loss cone by orders of magnitude because only principal $|n| = 1$ resonances operate. For higher electron energies (Figures 1(c), 1(d)) when $|n| > 1$ resonances start to operate, the pitch–angle scattering near the edge of the equatorial loss cone depends only slightly on the wave normal angle distribution, resulting in nearly the same bounce–averaged diffusion rate for all cases. In other words, there is an electron energy, depending on specified plasma and/or wave parameters, which separates lower and higher energy regions with different EMIC wave scattering properties. In the lower energy region, using a field–aligned wave normal angle distribution leads to a significant overestimate of the diffusion rate compared to oblique waves. In the higher energy region, the scattering rate near the edge of the loss cone almost does not depend on the wave normal angle distribution.

3. Local Pitch–Angle Diffusion Coefficient: CRRES Based Calculations

3.1. Minimum Resonant Energy

Recently, *Meredith et al.* [2003] presented an extensive statistical analysis of over 800 EMIC events observed on CRRES to establish whether electron scattering can occur at geophysically interesting energies (≤ 2 MeV). In the absence of specific information

on the wave normal angle, the dispersion relation for strictly field–aligned propagating EMIC waves was used to obtain the electron resonant energy. For consistency, *Meredith et al.* [2003] included only waves with a high ellipticity ($|\epsilon| \geq 0.3$) in the survey. This yielded a subset of 416 events, the majority of which were identified as L–mode. Considering only the central wave frequency, ω_m, in each wave packet, *Meredith et al.* [2003] found that in about 11 % of the observations, the electron minimum resonant energy fell below 2 MeV. These cases were restricted to regions where $\omega_{pe}/\Omega_e > 10$, and were associated with wave frequencies just below the helium or proton gyrofrequencies. More recently, trying to increase the above percentage, *Loto'aniu et al.* [2006] considered the entire frequency range for each of 25 EMIC wave packets observed on CRRES during the initial phase of a geomagnetic storm on 11 August, 1991. These authors also used the dispersion relation for strictly parallel propagating EMIC waves, and found that in comparison with results utilizing ω_m only, there are 3 to 4 times more wave packets that are able to interact with electrons below 2 MeV.

The minimum resonant energy depends on the wave normal angle, and the dependency is stronger in vicinity of the resonant frequencies where the wave number grows especially fast. Omitting the ω–term in a quasilinear resonance condition ($\omega - k_\parallel v_\parallel - n\Omega_e/\gamma = 0$) and taking $n = 1$, we can obtain the minimum kinetic energy required by electrons for cyclotron resonance interaction with EMIC waves,

$$\frac{E_{min}}{m_e c^2} = \frac{1}{\sqrt{1 - \left(\frac{v}{c}\right)^2}} - 1, \quad \left(\frac{v}{c}\right)^2 = \frac{1}{1 + \cos^2\theta \left(\frac{kc}{\Omega_e}\right)^2}, \tag{5}$$

where E_{min} is the minimum kinetic energy, m_e is the electron rest mass, c is the speed

of light, and k and v are the wave number and electron velocity. Note that equation (5) can be obtained from equation (7) of *Summers and Thorne* [2003] by omitting the two smallest terms in their equation. To calculate the electron minimum energy, we select the plasma parameters reported by *Loto'aniu et al.* [2006, Wave packet # 16], and the results of our calculation are presented in Figure 2. For $\theta = 0°$, as reported in many previous studies [e. g., *Summers and Thorne,* 2003], in order to get lower E_{min}, the required wave frequency has to be closer to the He^+ gyrofrequency (in other words, the wave number should be greater). For most wave normal angles, increasing the angle slightly also increases the minimum energy but there is a dramatic decrease of E_{min} in the region near $\theta = 90°$. This transition boundary depends on the wave frequency. Indeed, there is a resonant wave normal angle (the angle at which the wave number becomes infinite in the "cold plasma" approximation) for any frequency in the range between Ω_{He^+} and the corresponding bi–ion frequency, and this angle is closer to $\theta = 0°$ if the wave frequency is closer to Ω_{He^+}. Because of the wave number increase, the resonant energy decreases dramatically in the vicinity of the resonant wave normal angle, an effect clearly observed in Figure 2. So in cold plasma, E_{min} is lower for oblique or highly oblique wave propagation, depending on wave frequency, than for strictly field–aligned propagating EMIC waves. But, of course, the diffusion coefficient for those wave normal angles should be significant in order to determine the "physically meaningful" E_{min}, and moreover the cyclotron damping in vicinity of the He^+ gyrofrequency can be very strong (see below).

Figure 2

3.2. Pitch–Angle Diffusion Coefficient

It was demonstrated in section 2 that oblique wave propagation can strongly change the effectiveness of both the local and bounce–averaged relativistic electron scatterings. At the same time, those results were obtained for plasma parameters and wave spectra which were specified independently. So it is important to consider the effect of using concurrent observational data. In contrast to section 2, we now calculate the local pitch–angle diffusion coefficients using the data for plasma and wave parameters reported by *Loto'aniu et al.* [2006].

A long duration wave event was observed by CRRES on 11 August, 1991 in the interval $\sim 0500 - 0700$ UT (14.4 – 15.8 MLT) over a magnetic latitude range of $-26°$ to $-24°$ and L=6.3–7.6. CRRES was close to apogee in the plasmatrough, and the electron density varied slowly from 12 to 17 cm^{-3}. A total of 25 EMIC wave packets were identified both below and above the local He^+ gyrofrequency [*Loto'aniu et al.*, 2006]. In order to estimate the spectral properties of the wave packets, these authors fitted a Gaussian distribution to the static wave packet transverse power spectral density. Typical FFT data windows and frequency resolutions for the static spectrograms were 100 s and 0.02 Hz, respectively. The Gaussian function fit provided the central frequencies, ω_m, and the spectral semibandwidths, $\delta\omega$. The total wave magnetic power, δB^2, was estimated for each wave packet by summing the power spectral density bins in the range $\omega_m \pm \delta\omega$ and then multiplying the result by $\delta\omega$. Using the full wave spectral range, *Loto'aniu et al.* [2006] found that electrons with $E \leq 2$ MeV could interact with

only three wave packets (16, 17, and 19) if stormtime ion concentration was assumed (70% H^+, 20% He^+, and 10% O^+). Those packets were the He^+–mode EMIC waves, and for the calculation below we selected two of them. The associated plasma and wave characteristics are summarized in Table 1. Note that to generate this Table we used the definition of full–width at half maximum (FWHM) as it was given by *Loto'aniu et al.* [2006], i. e., FWHM $= 2\sqrt{2\ln 2}\delta\omega$, despite the Gaussian fit $\sim \exp\left\{-\left(\omega-\omega_m\right)^2/\delta\omega^2\right\}$. Of the packets 16, 17, and 19, wave packet 16 has the most narrow and 19 the widest distributions, with corresponding power spectral densities presented in Figure 3.

Table 1

Figure 3

To show the effect of the wave normal angle distribution on relativistic electron scattering, we use the wave normal angle distributions (2), and in addition, a stormtime ion concentration is assumed. For reference purposes, we also calculate the diffusion coefficients for strictly parallel/antiparallel propagating EMIC waves. For each wave packet, the power spectral density is normalized to the corresponding wave magnetic power δB^2 shown in Table 1, and this normalization is kept the same for any particular wave normal angle distribution (2). In order to estimate the minimum resonant energy we use y_{UC} from Table 1. For strictly field–aligned wave propagation, as follows from Figure 2, the energy is about 2 MeV for both wave packets (we can use Figure 2 for wave packet 19 because ω_{pe}/Ω_e was nearly the same during both). This minimum resonant energy exceeds the values presented by *Loto'aniu et al.* [2006], especially for wave packet 16; for this packet and a stormtime ion concentration, they obtained $E_{min} = 0.2$ MeV that, as follows from Figure 2, corresponds to a y_{UC} about 0.2496.

Figure 4 shows the results of our calculation for wave packet 16. For strictly

Figure 4

parallel wave propagation the minimum resonant energy is only slightly below 2 MeV, and the diffusion coefficients for field–aligned and intermediate wave propagation are only nonzero in Figures 4(c) and 4(d). Cases A and B demonstrate results similar to Figures 1(b) and 1(c). Because y_{UC} is very close to the He^+ gyrofrequency, the minimum resonant energy falls below 1 MeV if the wave normal angle exceeds 88°, so that Case C may potentially scatter such low energy electrons with an appreciable rate as shown in Figures 4(a) and 4(b). Another feature of highly oblique waves is clearly observed in Figures 4(d) where the range of pitch–angle diffusion is substantially extended down to the loss cone. While Case C exhibits a quite different behavior compared to Figure 1, there is a similarity between the diffusion coefficients in Figures 4(d) and 1(c).

The diffusion coefficients for wave packet 19 are shown in Figure 5. Both Figure 5(c) and 5(d) are quite similar, and demonstrate qualitatively the same behavior as in Figures 1(a) and 1(b). As follows from Figures 5(a) and 5(b), Case C practically does not scatter low energy electrons, mainly because of a lower y_{UC} for wave packet 19 than in Figure 4.

Figure 5

3.3. Cyclotron Damping Near He^+ Gyrofrequency and Its Consequence for Electron Scattering

As follows from Table 1, y_{UC} is very close to the local He^+ gyrofrequency ($y_{He^+} = 0.25$) for both wave packets. In this frequency region, the He^+–mode experiences strong cyclotron damping due to interaction with thermal He^+ [e. g., *Akhiezer et al.*, 1975]. To demonstrate this, we assume the He^+ temperature to be

$T_{He^+} = 1$ eV, and present in Figure 6 the wave damping rate for the stormtime ion composition and plasma parameters observed during wave packet 16. The frequency range shown covers approximately the entire wave packet 16. The damping rate for y_{LC} has only narrow peak for $\theta > 89°$, and this region is excluded from the calculation of the diffusion coefficients (see equation (2)). For y_m, the region of damping near ninety degrees extends slightly below 89°, and in addition, small damping appears for a field–aligned wave propagation. The situation becomes dramatically different for y_{UC} when the He^+–mode experiences strong damping in the entire wave normal angle region; the energy damping rate is $0.5/\gamma_{He^+} \approx 7$ sec, which is only four times greater than the wave period. In all cases, substantial damping takes place only if $|y - 0.25| \lesssim k_{\|} v_{\|,He^+}/\Omega_{H^+}$, where $v_{\|,He^+}$ is the field–aligned temperature of He^+. Moreover, we employ a "cold plasma" approximation in our diffusion coefficient software (as was done by *Loto'aniu et al.* [2006]), some must check the validity of this approximation. Particularly, the inequality

Figure 6

$$|y - 0.25| >> \frac{k_{\|} v_{\|,He^+}}{\Omega_{H^+}} = \varepsilon_{th} \tag{6}$$

should hold.

Inequality (6) is extremely crucial for the diffusion coefficient calculation because thermal effects should be considered if inequality (6) is violated, but more importantly, the He^+–mode damps strongly in the region $|y - 0.25| \lesssim \varepsilon_{th}$. For wave packets 16 and 19, inequality (6) is strongly violated in the vicinity of y_{UC}, and waves cannot exist in these frequency regions, which for $T_{He^+} = 1$ eV, are the ranges $\varepsilon_{th} = 5 \times 10^{-3} - 9 \times 10^{-2}$

and $\varepsilon_{th} = 3 \times 10^{-3} - 6 \times 10^{-2}$, respectively. Using these numbers and Table 1, we conclude that in order to suppress cyclotron damping completely, the He^+ temperature should be decreased at least by 1/80 for wave packet 16, and at least by 1/40 for wave packet 19. Any reasonable change to the temperature assumed in our calculation cannot eliminate the effect, and can only influence the frequency range subject to cyclotron damping.

Our conclusion that EMIC waves experience strong cyclotron damping near the He^+ gyrofrequency contradicts the results of *Loto'aniu et al.* [2006] because these authors estimated all their y_{UC} values from CRRES data (after filtering, FFT, and Gaussian approximations). Unfortunately we do not know all the details regarding data processing used by *Loto'aniu et al.* [2006], but we know that the wave frequency resolution in their data was 0.02 Hz. This uncertainty provides the ranges $(y_{LC}, y_{UC}) = (0.20 - 0.25, 0.22 - 0.27)$ and $(y_{LC}, y_{UC}) = (0.17 - 0.22, 0.22 - 0.27)$ for wave packets 16 and 19, respectively, that can reconcile our theoretical result with data reported by *Loto'aniu et al.* [2006]. So we do not see any reason inequality (6) is violated, and it must be taken into account.

Let us now recalculate the diffusion coefficients presented in Figure 4, neglecting contributions from all the partial diffusion coefficients if $|y - 0.25| \leq \varepsilon_{th}$ (keeping all parameters the same). Note that all the results presented in Figure 1 are still valid because inequality (6) holds for all those parameters. The results of the recalculation are presented in Figure 7, and there is a qualitative difference in comparison to Figure 4. Now, for all wave normal angle distributions, low energy electron pitch–angle diffusion

290 is not possible, and while the 2 MeV diffusion coefficients are nonzero in Figure 7(c),
291 they are at least partly inside the equatorial loss cone for L $\approx$ 7.3. For greater electron
292 energies, the contribution from the high frequency part of the wave power spectral
293 density decreases. As a result, Figures 7(d) and 4(d) look similar except that diffusion
294 vanishes at slightly lower pitch–angles in Figure 7(d) than in Figure 4(d), and the
295 transition between $|n| = 1$ and $|n| = 2$ resonances is not continued in Figure 7(d) for
296 Case A.

297 The results of our recalculation for wave packet 19 are shown in Figure 8. Similar Figure 8
298 to wave packet 16, diffusion is not possible for low energies, and Figures 8(d) and 5(d)
299 are very similar.

300 In conclusion, we emphasize that as we demonstrated above, the He^+–mode
301 does not experience significant cyclotron damping by thermal He^+ if $y \lesssim y_m$ (see
302 Figure 6). So the observed changes in the diffusion coefficients are due to the frequency
303 region near y_{UC}, and qualitatively correct diffusion coefficients may be obtained by
304 only considering the region $y \lesssim y_m$. This result is consistent with the conclusions of
305 *Meredith et al.* [2003] regarding the electron minimum resonant energy which were
306 obtained by considering only the central wave packet frequencies, and suggests that the
307 number of EMIC wave packets that are able to interact with electrons below 2 MeV
308 may significantly decrease compared with the estimate of *Loto'aniu et al.* [2006].

4. Summary and Conclusions

Precipitation of outer RB electrons due to resonant pitch–angle scattering by EMIC waves is considered to be one of the most important loss mechanisms. The effectiveness of relativistic electron scattering depends strongly on the EMIC wave spectral properties, but unrealistic assumptions regarding the wave angular spread were made in previous theoretical studies. Namely, only strictly field–aligned or quasi field–aligned waves were considered [*Summers and Thorne,* 2003; *Albert,* 2003; *Loto'aniu et al.,* 2006]. The effect of oblique EMIC waves on relativistic electron scattering was recently discussed by *Glauert and Horne* [2005]. For prescribed plasma and wave parameters, considering the H^+–mode EMIC waves, they calculated the local diffusion coefficients and demonstrated that when a realistic angular spread of propagating waves is taken into account, electron diffusion at ~ 0.5 MeV is only slightly reduced compared with the assumption of field–aligned propagation, but at ~ 5 MeV, electron diffusion at pitch–angles near 90° is reduced by a factor of 5 and increased by several orders of magnitude at pitch–angles $30° - 80°$. Thus at energies of a few MeV the assumption of field–aligned wave propagation breaks down, significantly overestimates the pitch–angle diffusion coefficient at large pitch–angles, and underestimates the local diffusion rate at smaller pitch–angles by orders of magnitude.

The purpose of the present study was to consider the impact of oblique EMIC waves on local relativistic electron scattering using simultaneous observations of plasma and wave parameters from CRRES, and to estimate the effect of bounce averaging.

Analyzing 25 EMIC wave packets, and considering the full wave spectral range, *Loto'aniu et al.* [2006] found that electrons with $E \leq 2$ MeV could interact with wave packets 16, 17, and 19 only if a stormtime ion concentration is assumed (70% H^+, 20% He^+, and 10% O^+). Those packets were He^+–mode EMIC waves, where we have selected wave packets 16 and 19 for our analyzes. Results of our study can be summarized as follows:

1. In comparison with the field–aligned waves, the intermediate and highly oblique distributions slightly decrease the pitch–angle range subject to diffusion, and reduce the local scattering rate by about an order of magnitude at pitch–angles where the principle $|n| = 1$ resonances operate (see Figures 7 and 8). Oblique waves allow the $|n| > 1$ resonances to operate, extending the range of local pitch–angle diffusion down to the loss cone, and increasing the diffusion at lower pitch–angles by orders of magnitude (see Figures 7(d)).

2. The local diffusion coefficients based on concurrent plasma/wave parameters from CRRES are qualitatively similar to the results obtained for defined plasma parameters with model wave spectra (compare Figures 7 and 8 with the first row in Figure 1). So we anticipate that the bounce–averaged diffusion coefficients, if estimated from concurrent wave/particle data, will exhibit dependencies similar to those we found for the model bounce–averaged calculations (see Figure 1, the third row). Those dependencies are:

3. For low energy electrons, if only principal $|n| = 1$ resonances operate, intermediate and highly oblique wave distributions (in contrast to field–aligned waves) reduce the equatorial pitch–angle range subject to diffusion, and decrease the bounce–averaged

scattering rate near the edge of the equatorial loss cone by orders of magnitude. This low energy threshold depends on specified plasma and/or wave parameters, which is $E \approx 2$ MeV for parameters used in Figure 1.

4. For greater electron energies, the $|n| = 1$ resonances operate only in a narrow region at large pitch-angles (see Figures 1(c) and 1(d)), but due to significant scattering at higher latitudes, the bounce–averaged diffusion coefficients for field–aligned waves extend down to the equatorial loss cone. For these energies, oblique waves operating at $|n| > 1$ resonances are more effective and provide nearly the same bounce–averaged scattering rate in the vicinity of the loss cone as field–aligned waves do (see Figures 1(c) and 1(d), the third row).

Acknowledgments. This research was performed while K. Gamayunov held a NASA Postdoctoral Program appointment at NASA/MSFC. Funding in support of this study was provided by NASA grant UPN 370–16–10, NASA HQ POLAR Project, and NASA LWS Program.

References

Akhiezer, A. I., I. A. Akhiezer, R. V. Polovin, A. G. Sitenko, and K. N. Stepanov (1975), *Plasma Electrodynamics,* vol. 1, Pergamon, Tarrytown, N. Y.

Albert, J. M. (2003), Evaluation of quasi–linear diffusion coefficients for EMIC waves in a multispecies plasma, *J. Geophys. Res., 108,* A6, 1249, doi:10.1029/2002JA009792.

Foat, J. E., R. P. Lin, D. M. Smith, F. Fenrich, R. Millan, I. Roth, K. R. Lorentzen, M. P. McCarthy, G. K. Parks, and J. P. Treilhou (1998), First detection of a terrestrial MeV X–ray burst, *Geophys. Res. Lett., 25,* 4109.

Glauert, S. A., and R. B. Horne (2005), Calculation of pitch angle and energy diffusion coefficients with the PADIE code, *J. Geophys. Res., 110,* A04206, doi:10.1029/2004JA010851.

Green, J. C., T. G. Onsager, T. P. O'Brien, and D. N. Baker (2004), Testing loss mechanisms capable of rapidly depleting relativistic electron flux in the Earth's outer radiation belt, *J. Geophys. Res., 109,* A12211, doi:10.1029/2004JA010579.

Khazanov, G. V., K. V. Gamayunov, D. L. Gallagher, and J. U. Kozyra (2006), Self–consistent model of magnetospheric ring current and propagating electromagnetic ion cyclotron waves: Waves in multi ion magnetosphere, *J. Geophys. Res., 111,* A10202, doi:10.1029/2006JA011833.

Khazanov, G. V., K. V. Gamayunov, D. L. Gallagher, J. U. Kozyra, and M. W. Liemohn (2007), Self–consistent model of magnetospheric ring current and propagating electromagnetic ion cyclotron waves. 2. Wave induced ring current

precipitation and thermal electron heating, *J. Geophys. Res., 112,* A04209, doi:10.1029/2006JA012033.

Khazanov, G. V., K. V. Gamayunov, and V. K. Jordanova, Self–consistent model of magnetospheric ring current ions and electromagnetic ion cyclotron waves: The 2–7 May 1998 storm (2003), *J. Geophys. Res., 108*, A12, 1419, doi:10.1029/2003JA009856.

Kim, H.–J., and A. A. Chan, Fully adiabatic changes in storm time relativistic electron fluxes (1997), *J. Geophys. Res., 102,* 22107.

Li, X., D. N. Baker, M. Temerin, T. E. Cayton, G. D. Reeves, R. A. Christiansen, J. B. Blake, M. D. Looper, R. Nakamura, and S. G. Kanekal (1997), Multi–satellite observations of the outer zone electron variation during the November 3–4, 1993, magnetic storm, *J. Geophys. Res., 102,* 14123.

Lorentzen, K. R., M. P. McCarthy, G. K. Parks, J. E. Foat, R. M. Millan, D. M. Smith, R. P. Lin, and J. P. Treilhou (2000), Precipitation of relativistic electrons by interaction with electromagnetic ion cyclotron waves, *J. Geophys. Res., 105,* 5381.

Loto'aniu, T. M., R. M. Thorne, B. J. Fraser, and D. Summers (2006), Estimating relativistic electron pitch angle scattering rate using properties of the electromagnetic ion cyclotron wave spectrum, *J. Geophys. Res., 111,* A04220, doi:10.1029/2005JA011452.

Lyons, L. R., and R. M. Thorne (1972), Parasitic pitch angle diffusion of radiation belt particles by ion cyclotron waves *J. Geophys. Res., 77,* 5608.

409 Meredith, N. P., R. B. Horne, D. Summers, R. M. Thorne, R. H. A. Iles, D. Heynderickx,
410 and R. R. Anderson (2002), Evidence for acceleration of outer zone electrons to
411 relativistic energies by whistler mode chorus, *Ann. Geophys., 20,* 967.
412 Meredith, N. P., R. M. Thorne, R. B. Horne, D. Summers, B. J. Fraser, and R. R.
413 Anderson (2003), Statistical analysis of relativistic electron energies for cyclotron
414 resonance with EMIC waves observed on CRRES, *J. Geophys. Res., 108,* A6,
415 1250, doi:10.1029/2002JA009700.
416 Millan, R. M., R. P. Lin, D. M. Smith, K. R. Lorentzen, and M. P. McCarthy (2002), X–
417 ray observations of MeV electron precipitation with a balloon–borne germanium
418 spectrometer, *Geophys. Res. Lett., 29*(24), 2194, doi:10.1029/2002GL015922.
419 Reeves, G. D., K. L. McAdams, R. H. W. Friedel, and T. P. O'Brien (2003), Acceleration
420 and loss of relativistic electrons during geomagnetic storms, *Geophys. Res. Lett.,*
421 *30*(10), 1529, doi:10.1029/2002GL016513.
422 Shprits, Y. Y., W. Li, and R. M. Thorne (2006), Controlling effect of the pitch angle
423 scattering rates near edge of the loss cone on electron lifetimes, *J. Geophys. Res.,*
424 *111,* A12206, doi:10.1029/2006JA011758.
425 Summers, D., C. Ma, and T. Mukai (2004), Competition between acceleration and loss
426 mechanisms of relativistic electrons during geomagnetic storms, *J. Geophys. Res.,*
427 *109,* A04221, doi:10.1029/2004JA010437.
428 Summers, D., B. Ni, and N. P. Meredith (2007), Timescales for radiation belt electron
429 acceleration and loss due to resonant wave–particle interactions: 2. Evaluation
430 for VLF chorus, ELF hiss, and electromagnetic ion cyclotron waves, *J. Geophys.*

Res., 112, A04207, doi:10.1029/2006JA011993.

Summers, D., and R. M. Thorne (2003), Relativistic electron pitch–angle scattering by electromagnetic ion cyclotron waves during geomagnetic storms, *J. Geophys. Res., 108,* A4, doi:10.1029/2002JA009489.

Thorne, R. M., and R. B. Horne (1992), The contribution of ion–cyclotron waves to electron heating and SAR–arcs excitation near the storm–time plasmapause, *Geophys. Res. Lett., 19,* 417.

Thorne, R. M., R. B. Horne, S. A. Glauert, N. P. Meredith, Y. Y. Shprits, D. Summers, and R. R. Anderson (2005), The influence of wave–particle interactions on relativistic electron dynamics during storms, in *Inner Magnetosphere Interactions: New Perspectives From Imaging, Geophys. Monogr. Ser.,* vol. 159, edited by J. Burch, M. Schulz, and M. Spence, pp. 101–112, AGU, Washington, D. C.

Thorne, R. M., and C. F. Kennel (1971), Relativistic electron precipitation during magnetic storm main phase, *J. Geophys. Res., 76,* 4446.

K. V. Gamayunov, National Space Science and Technology Center, NASA Marshall Space Flight Center, Space Science Department, 320 Sparkman Drive, Huntsville, AL 35805, USA. (e–mail: konstantin.gamayunov@msfc.nasa.gov)

G. V. Khazanov, National Space Science and Technology Center, NASA Marshall Space Flight Center, Space Science Department, 320 Sparkman Drive, Huntsville, AL 35805, USA. (e–mail: george.khazanov@msfc.nasa.gov)

452 Received _____

Figure 1. Equatorial and bounce–averaged diffusion coefficients versus equatorial pitch–angle for scattering relativistic electrons by the He^+–mode of EMIC waves. Spectral parameters and ion content are given in the text. L=4, and $(\omega_{pe}/\Omega_e)^2 = 10^3$, where ω_{pe} and Ω_e are the equatorial electron plasma frequency and gyrofrequency (without Lorentz factor), respectively. The curve "Gauss" is for a wave normal angle distribution adopted by *Albert* [2003]. The second row shows the average resonant number weighted by the partial equatorial diffusion coefficient (see the text for definition).

Figure 2. Minimum resonant energy versus normal angle of the He^+–mode EMIC waves. The plasma density and magnetic field are 17 cm^{-3} and 171 nT, taken from [*Loto'aniu et al.*, 2006, Wave packet # 16]. The ion composition is 70% H^+, 20% He^+, and 10% O^+, and the normalized wave frequency is defined as $y = \omega/\Omega_{H^+}$.

Figure 3. Transverse power spectral densities for wave packets 16 and 19 obtained by *Loto'aniu et al.* [2006]. The solid and dashed vertical lines restrict the frequency range $\omega_m \pm \delta\omega$ for packets 16 and 19, respectively.

Figure 4. Local pitch–angle diffusion coefficients for wave packet 16. Calculations are based on a stormtime ion composition, $\eta_{H^+} = 0.7$, $\eta_{He^+} = 0.2$, and $\eta_{O^+} = 0.1$. "W/P 16" shows the results for strictly parallel–antiparallel propagating He^+–modes, and Cases A, B, and C are obtained for the corresponding wave normal angle distribution given by (2).

Figure 5. Same as Figure 4, except for wave packet 19.

Figure 6. The He^+–mode damping rate due to interaction with thermal He^+. The phase space distribution function for He^+ is Maxwellian with $T_{He^+} = 1$ eV, but thermal effects are neglected in the real part of the dispersion relation. All other plasma species are described in a "cold plasma" approximation. A stormtime ion composition is assumed, and the plasma density and magnetic field are taken from [*Loto'aniu et al.,* 2006, Wave packet # 16].

Figure 7. Same as Figure 4, except inequality $|y - 0.25| > k_{\|} v_{\|,He^+}/\Omega_{H^+}$ is held during the diffusion coefficient calculations.

Figure 8. Same as Figure 5, except inequality $|y - 0.25| > k_{\|} v_{\|,He^+}/\Omega_{H^+}$ is held during the diffusion coefficient calculations.

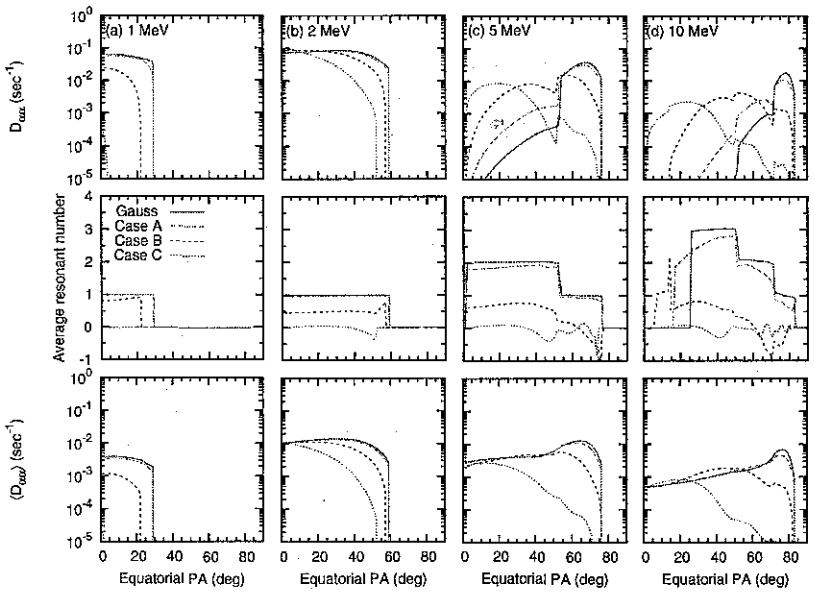

461

462 **Figure 1.**

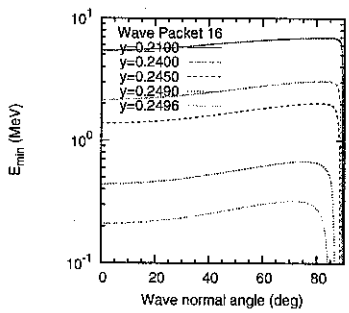

463

464 **Figure 2.**

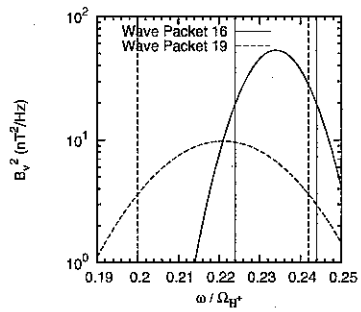

465

466 **Figure 3.**

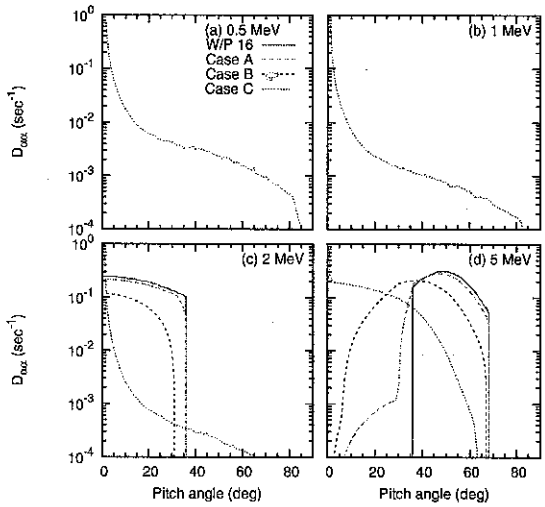

467

468 **Figure 4.**

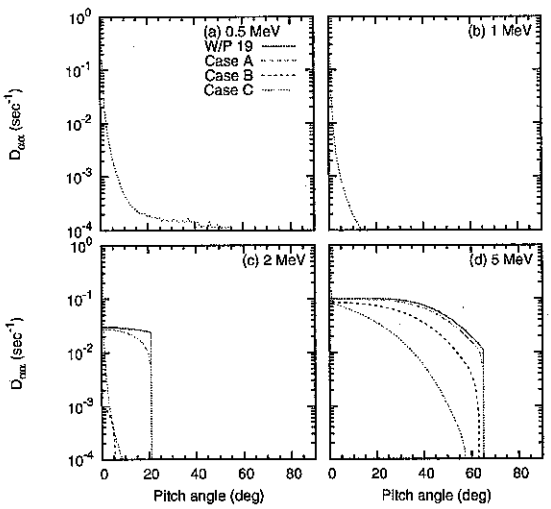

469

470 **Figure 5.**

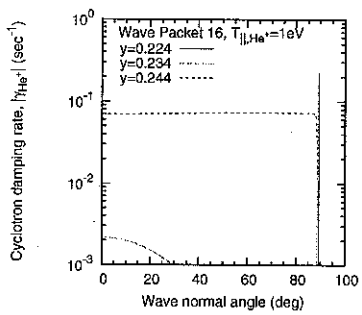

471

472 **Figure 6.**

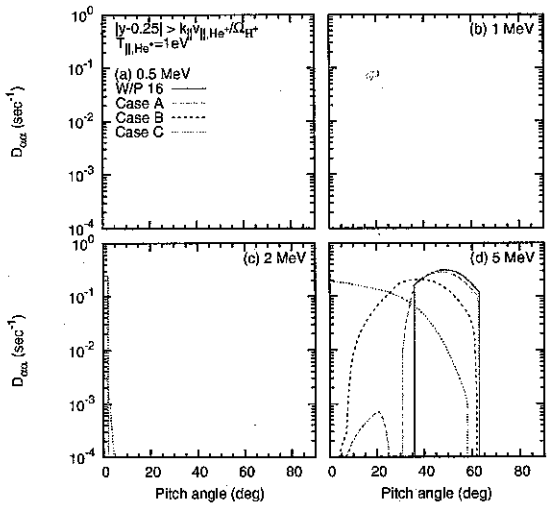

473

474 **Figure 7.**

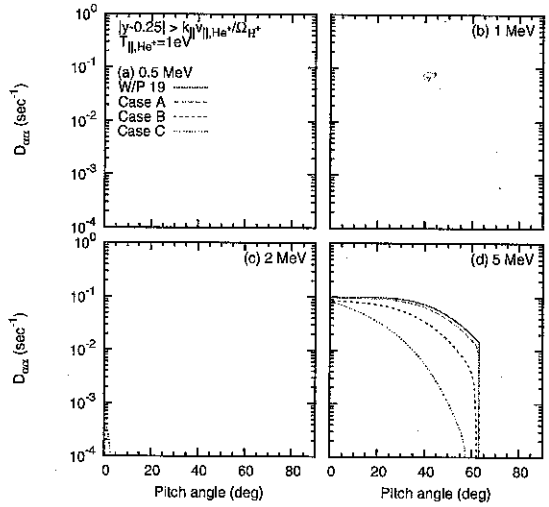

475

476 **Figure 8.**

Table 1. Wave Packet and Local Environment Properties Selected From [*Loto'aniu et al.*, 2006]

Wave Packet	$y_m = \omega_m/\Omega_{H+}$	$\delta y = \delta\omega/\Omega_{H+}$	$y_{LC} = y_m - \delta y$	$y_{UC} = y_m + \delta y$	δB^2 nT^2	B_0 nT	N_e cm^{-3}
16	0.23	0.01	0.22	0.24	2.21	170.9	17
19	0.22	0.02	0.20	0.24	0.84	160.2	15